Published in final edited form as:
Cancer Res. 2017 November ; 77(21): 5913–5924. doi:10.1158/0008-5472.CAN-16-2686.

MCT1 inhibitor AZD3965 increases mitochondrial metabolism, facilitating combination therapy and non-invasive magnetic resonance spectroscopy

Mounia Beloueche-Babari[1], **Slawomir Wantuch**[1], **Teresa Casals Galobart**[1], **Markella Koniordou**[1], **Harold G Parkes**[1], **Vaitha Arunan**[1], **Yuen-Li Chung**[1], **Thomas R Eykyn**[1], **Paul D Smith**[2], and **Martin O Leach**[1]

[1]Cancer Research UK Cancer Imaging Centre, Division of Radiotherapy and Imaging, The Institute of Cancer Research, London and The Royal Marsden NHS Foundation Trust, SM2 5PT, UK

[2]AstraZeneca, Cancer Biosciences, Cancer Research UK Cambridge Institute, Cambridge, CB2 0RE UK

Abstract

Monocarboxylate transporters (MCT) modulate tumor cell metabolism and offer promising therapeutic targets for cancer treatment. Understanding the impact of MCT blockade on tumor cell metabolism may help develop combination strategies or identify pharmacodynamic biomarkers to support the clinical development of MCT inhibitors now in clinical trials. In this study, we assessed the impact of the MCT1 inhibitor AZD3965 on cancer cell metabolism *in vitro* and *in vivo*. Exposing human lymphoma and colon carcinoma cells to AZD3965 increased MCT4-dependent accumulation of intracellular lactate, inhibiting monocarboxylate influx and efflux. AZD3965 also increased the levels of TCA cycle-related metabolites and ^{13}C-glucose mitochondrial metabolism, enhancing oxidative pyruvate dehydrogenase and anaplerotic pyruvate carboxylase fluxes. Increased mitochondrial metabolism was necessary to maintain cell survival under drug stress. These effects were counteracted by co-administration of the mitochondrial complex I inhibitor metformin and the mitochondrial pyruvate carrier inhibitor UK5099. Improved bioenergetics were confirmed *in vivo* after dosing with AZD3965 in mouse xenograft models of human lymphoma. Our results reveal new metabolic consequences of MCT1 inhibition that might be exploited for therapeutic and pharmacodynamic purposes.

Keywords

cancer metabolism; MCT1; combination therapy; non-invasive biomarkers

Correspondence: Mounia Beloueche-Babari (mounia.beloueche-babari@icr.ac.uk, phone: +44 2086613728, fax: +44 2086610846) Cancer Research UK Cancer Imaging Centre, Division of Radiotherapy and Imaging, The Institute of Cancer Research, London and The Royal Marsden NHS Foundation Trust, Downs Road, Sutton, Surrey SM2 5PT, United Kingdom.

Introduction

Metabolic “re-wiring” is a hallmark of cancer that enables malignant cells to meet their growth demands, survive and thrive in a hostile tumor microenvironment. The Warburg effect, describes tumor cell preferential use of the glycolytic pathway to generate lactate under aerobic conditions. This process leads to excess production of lactate, which is removed from cells via monocarboxylate transporters (MCTs), a family of transmembrane proteins (including MCT1, MCT2, MCT3 and MCT4) that mediate the proton-linked bi-directional movement of lactate (as well as pyruvate and ketone bodies) in and out of cells (1). The excreted lactate not only prevents intracellular acidification-driven cell toxicity but is believed to aid in tumor invasion, immune suppression as well as providing lactate as a fuel source for the more oxidative neighboring tumor cells (2–4).

MCT1 and MCT4 are overexpressed in cancer and disrupting lactate transport represents a promising approach for antineoplastic therapeutic targeting (2,4–6). Indeed, several inhibitors of MCT1 have recently been described that have shown promising pre-clinical activity, including the dual MCT1/MCT2 inhibitor AR-C155858 (5) and the MCT1 inhibitors SR13800 (7) and AZD3965 (8).

AZD3965 is a selective MCT1 inhibitor that exhibits some activity against MCT2 (but not MCT3 or MCT4), showing growth-inhibitory activity in human gastric and small cell lung cancer tumor xenografts *in vivo* (8,9). AZD3965 is currently in phase I and progressing to phase II clinical trials in the UK (www.clinicaltrials.gov) and understanding its impact on cellular metabolism as well as identifying pharmacodynamic (PD) biomarkers for MCT1 modulation is much needed for furthering the clinical development of this and other MCT1-targeted drugs.

In this context, metabolic profiling approaches enable the interrogation of tumor metabolism and, as such, lend themselves to PD biomarker discovery and evaluation of anti-cancer drugs targeting metabolism, including AZD3965. NMR spectroscopy is one technique that enables the steady state and dynamic assessment as well as *in vivo* study of cellular metabolism. The technique has shown great promise for mechanism-based PD metabolic biomarker discovery following targeted cancer therapy, facilitating the translation of studies from experimental cancer models through to patients (10–12). For example, depletion of hexokinase-2 and CMYC following treatment with a MEK inhibitor in BRAF-driven human melanoma cells and xenograft tumors resulted in decreased lactate levels as observed with ^{1}H NMR (13). Further, PI3K inhibitor-mediated depletion of lactate dehydrogenase (LDH) expression led to a fall in hyperpolarized ^{13}C-pyruvate-lactate exchange, assessed by dynamic ^{13}C NMR of human cancer cells and tumors (14,15).

MCT1 inhibition with AZD3965 has been shown to activate glycolytic metabolism, increasing glycolytic intermediate levels (e.g. glucose 6-phosphate and fructose 6-phosphate) as well as enzyme activity (e.g. hexokinase and pyruvate kinase) concomitant with intracellular lactate ($Lactate_I$) accumulation (9). However, a recent study in human breast cancer cells showed that AZD3965 has no impact on glycolytic activity or $Lactate_I$ and that its anti-tumor effects are due to inhibition of pyruvate export (16). It is not clear

whether the discrepancies in reported effects are due to variations in baseline MCT4 levels, how AZD3965 affects downstream metabolic pathways and fluxes, and whether any of the drug-induced metabolic changes could have potential as non-invasive PD biomarkers of target inhibition.

In this study, using human lymphoma and colon carcinoma cells with varying baseline MCT4 expression, we show that AZD3965 inhibits monocarboxylate transport in and out of cells concomitant with increased bioenergy-related metabolite levels in MCT4- as well as MCT4+ cells. The latter effect is attributed to activation of mitochondrial metabolism via oxidative pyruvate dehydrogenase (PDH) flux, which was accompanied by a relative increase in anaplerotic pyruvate carboxylase (PC) flux. The increased mitochondrial metabolism enabled continued cell survival under drug treatment which was prevented by co-administration of the mitochondrial complex I inhibitor metformin and pyruvate carrier inhibitor UK5099. Our data also show that the improved bioenergetics are detectable in a tumor xenograft model, using *in vivo* ^{31}P NMR spectroscopy, indicating potential for non-invasive evaluation of drug action.

Materials and Methods

Cell lines and reagents

Raji and Hut78 human lymphoma cells were purchased from ATCC. Kelly and IMR-32 human neuroblastoma and HT29 human colon carcinoma cells were originally obtained from ATCC and authenticated in our laboratory using STR profiling on 16th October 2015 and 13th March 2017, respectively. Lymphoma and neuroblastoma cells were grown in RPMI while HT29 cells were grown in DMEM as previously described (17). These cell lines were chosen to provide a range of baseline expression of MCT4, with lymphomas being also a target for the phase I trial expansion cohort and neuroblastoma (*MYCN*-amplified) representing a solid tumor type expected to be MCT1-dependent (7). AZD3965 was provided by AstraZeneca, UK. Metformin and UK5099 were purchased from Sigma-Aldrich (Dorset, UK).

Cell counts and growth inhibition assays

Cell counts were obtained using a Beckman Coulter Vi-Cell® Cell Viablity Analyzer. Drug treatment effects on growth were determined using a CellTiter-Blue® Viability assay (Promega; Southampton, UK) following 72h incubation, or by cell counting after 24h, 48 and 72h treatment using Trypan blue exclusion of dead cells.

In vitro cell treatments

Cells were treated with either DMSO (0.01%) or AZD3965 at the indicated concentrations in fresh media and cells and/or spent media collected at the indicated time points for analysis. To assess changes in glucose metabolism, cells were incubated in media containing 100% 5mM [1-^{13}C]glucose for 6h in drug or DMSO, followed by cell and culture media collection for ^{13}C NMR.

In vivo animal model

Raji xenograft tumors were established by subcutaneous injection of $5x10^6$ Raji cells in 0.1ml of a 1:1 medium:matrigel solution into the flank of female SCID mice (6-8 weeks old). Tumors were measured as previously described (17) and once they reached ~450 mm^3 in volume (after ~3-4 weeks), mice were randomized into two groups; one group was treated with vehicle (85% saline, 10% DMSO and 5% tween (n=7)) and the other with 50 mg/kg AZD3965 dissolved in vehicle (n=6) administered orally twice daily, a schedule based on a previously published report (8). For *in vivo* NMR spectroscopy, mice received three doses in total: 2 doses on day 1 and one dose on day 2. For growth inhibition measurements, a separate cohort of mice bearing tumors of ca. $350mm^3$ in volume was treated with either vehicle (n=4) or AZD3965 (n=3) as above for a total of 5 days and tumor volume monitored. All experimental protocols were monitored and approved by the ICR Animal Welfare and Ethical Review Body Animal Welfare and Ethical Review Body, in accordance with UK Home Office regulations under the Animals (Scientific Procedures) Act 1986 and UK National Cancer Research Institute (NCRI) Guidelines for the Welfare and Use of Animals in Cancer Research (18).

In vivo NMR spectroscopy

Mice were anesthetized as previously described (17) and placed at the isocenter of a horizontal Bruker 7 Tesla microimaging system (Bruker Instruments, Ettlingen, Germany) with the tumors positioned in the centre of a 15 cm dual tune $^1H/\ ^{31}P$ surface coil. After shimming (achieving a linewidth on the unsuppressed water peak of ~20 Hz on average), localized image-selected ^{31}P NMR spectroscopy measurements of the tumors were performed prior to (day 0) and 2h hours following the last dose (on day 2). Data were processed using jMRUI and AMARES fitting to determine chemical shift positions and peak integrals as previously described (19). Intracellular tumor pH was calculated based on the chemical shift difference between the inorganic phosphate (Pi) and α-nucleotide triphosphate (α-NTP) peaks as previously reported (19). After the last scan, the experiment was terminated with a schedule 1 method and tumors excised, immediately snap-frozen in liquid nitrogen then stored at -80°C until further processing.

Metabolic assessment of cells and tumors

Cells and xenograft tumor tissue were extracted as previously described (20) and freeze-dried samples reconstituted in 540μl of D_2O containing 3-(trimethylsilyl) propionic-2,2,3,3-d_4 acid (TSP) as an internal ^1H NMR quantitation and chemical shift reference. For extracellular metabolite analysis, 1ml of media was freeze-dried and reconstituted in D2O +TSP as above. ^{13}C NMR data were semi-quantified (AU/cell) relative to the TSP integral, using the [3-^{13}C] lactate peak at 21.4 ppm for chemical shift referencing. For ^{31}P NMR of cell extracts, 60μl of a D_2O solution containing EDTA and methylenediphosphonic acid (internal standard) to a final concentration of 10mM and 0.43mM respectively (pH 8.2) was added. Further details of data acquisition and processing are provided in Supplementary Methods.

Europe PMC Funders Author Manuscripts

In vitro hyperpolarized ^{13}C NMR

^{13}C-pyruvate-lactate exchange was monitored in intact Raji, Hut78 and HT29 human cancer cells exposed to DMSO or AZD3965 for 1h or 24h. For this, cell pellets (10-15x10^6 cells/sample) were washed in saline, incubated at 37°C in FBS-free medium and ^{13}C spectra acquired for 4 minutes with 2s intervals and a 10° pulse immediately after the addition of 10mM hyperpolarized [1-^{13}C]pyruvic acid and 10mM unlabeled lactate in a total volume of 0.5ml. Similar cell handling conditions were previously shown to be adequate for maintaining cell viability and metabolic activity (21) and to produce comparable data to perfused cell studies when looking at drug effects (14,22,23).

Dynamic hyperpolarized ^{13}C time-series spectra were summed and the ratio of the areas under the curve for the lactate and pyruvate peaks ($Lactate_{AUC}$/$Pyruvate_{AUC}$), a parameter shown to accurately reflect pyruvate-lactate exchange (22), was calculated.

Western blotting

Protein expression was performed using western blotting under standard conditions. Details of the primary and secondary antibodies are provided in Supplementary Methods.

Statistical analysis

A single comparison unpaired Student's t-test (for comparison of cell number and metabolite levels between control and treated cells) or a Wilcoxon matched-pairs signed rank test (for tumor volume and *in vivo* metabolite ratio changes prior to and following treatment) were used with $P<0.05$ considered statistically significant. Data represent the mean±SE.

Results

MCT1 inhibition with AZD3965 induces a concentration- and time-dependent accumulation of intracellular lactate in Raji human lymphoma cells

The direction of transport of lactate follows a lactate/H+ concentration gradient (1). In glycolytic cells incubated in fresh media, increased intracellular production of lactate favours export out of cells leading to accumulation upon MCT1 blockade (MCT1 being the dominant transporter in the absence of alternative transporters such as MCT4). Thus, prior to investigating the downstream metabolic effects of MCT1 inhibition, we assessed the impact of AZD3965 on $Lactate_I$, as an indicator of MCT1 blockade, in MCT4- Raji human lymphoma cells. We also examined the temporal dynamics of the response as well as its dependence on drug concentration.

Our data indicate that at 24h, AZD3965 induced accumulation of $Lactate_I$ that was observed with as little as 2nM AZD3965 (p=0.01) and became more pronounced with increasing drug concentrations, reaching a maximum at 25nM AZD3965 (figure 1A) and plateauing thereafter. Time course analysis with 25nM AZD3965 revealed rapid build-up of $Lactate_I$, showing a trend towards an increase as early as 15 minutes, becoming significant after 90 minutes (p=0.02), peaking at around 3h (up to 1890±230%, p=0.002) then showing a gradual decrease from 6h up to 72h post-treatment (p=0.03, Figure 1B). Extracellular lactate

($Lactate_E$) levels also decreased compared to control at 24h and up to 72h post-treatment (Figure 1C). Raji cell counts were reduced relative to control with exposure to AZD3965, however cell growth persisted despite the increase in $Lactate_I$ (Figure 1D) possibly suggesting activation of adaptive pathways.

Transport directionality and the relationship between MCT1 inhibition, $Lactate_I$ build-up and MCT4 expression

We next tested whether AZD396 also inhibited MCT1-mediated substrate transport into cells, and the relationship between $Lactate_I$ accumulation and MCT1 inhibition in the presence or absence of MCT4, an alternative mediator of lactate efflux and a predictor of resistance to AZD3965 (8). For this, we used MCT4- Raji cells and two additional human cancer cell lines expressing varying levels of MCT4: Hut78 lymphoma (low MCT4: MCT4+) and HT29 colon carcinoma (high MCT4: MCT4+++), Figure 2A.

24h exposure to a low concentration of AZD3965 (5nM) led to a 10-fold build-up in $Lactate_I$ in MCT4+ Hut78 human lymphoma cells, which was sustained at higher drug concentrations (25nM and 500nM), Figure 2B. In contrast, MCT4+++ HT29 human colon carcinoma cells showed a trend towards an increase in $Lactate_I$ relative to controls with 5nM and 25nM AZD3965 which only became significant with exposure to 500 nM AZD3965 reaching up to 4-fold, relative to controls. i.e. much smaller in amplitude compared to Raji and Hut78 cells (Figure 2B). $Lactate_E$ levels were only marginally affected in MCT4+ Hut78 and MCT4+++ HT29 cells (Figure 2C), in keeping with the presence of the alternative lactate transporter MCT4.

To assess the effect of AZD3965 on monocarboxylate transport dynamics, we used hyperpolarized [1-^{13}C]pyruvate, also transported into cells via MCT1 (1), and monitored its exchange with lactate in our three cell lines.

Figure 2D shows representative ^{13}C spectra of summed data with signals from hyperpolarized ^{13}C-lactate, pyruvate and pyruvate hydrate and the time-dependent changes in hyperpolarized ^{13}C-lactate signals obtained from control and AZD3965-treated Raji cells. Representative time series spectra are also provided in Figure S1. Following 24h of treatment, the $Lactate_{AUC}/Pyruvate_{AUC}$ ratio, reflective of ^{13}C-pyruvate-lactate exchange (22), decreased in a concentration-dependent manner to 31±6% in 5nM AZD3965-treated and 19±2% in 25nM AZD3965-treated Raji cells relative to controls ($p<0.001$, n=6), indicating inhibition of [1-^{13}C]pyruvate uptake with AZD3965 (Figure 2E). Incubation of Raji cells for 1h with 25nM AZD3965 also reduced $Lactate_{AUC}/Pyruvate_{AUC}$ consistent with the immediate action of the drug on MCT1 (Figure 2E). Further, AZD3965 inhibited pyruvate-lactate exchange in MCT4+ Hut78 cells and in MCT4+++ HT29 cells even at drug concentrations that had no significant effect on intracellular lactate (Figure 2B, E), in line with MCT1-mediated transport of [1-^{13}C]pyruvate being a rate limiting step in the ^{13}C NMR observed reaction (24). MCT4+++ HT29 cells did however exhibit the smallest inhibition of pyruvate-lactate exchange, suggesting that the experimental conditions used may be permissive of some MCT4 mediated [1-^{13}C]pyruvate transport into cells.

Assay of the activity of LDH, the intracellular enzyme that catalyzes the conversion of pyruvate to lactate, showed no significant differences between control and AZD3965-treated Raji cells (Figure S2). Thus, the reduction in pyruvate-lactate exchange observed with AZD3965 appears to be driven primarily by reduced ^{13}C-pyruvate transport following MCT1 blockade.

These data confirm inhibition of MCT1 by AZD3965 in Raji, Hut78 and HT29 cells and indicate that the observed intracellular lactate build-up is a result of its decreased transport out of cells (and not increased influx), which is highly dependent on the near or complete absence of MCT4 expression.

AZD3965 alters cellular metabolism leading to an improved bioenergetic state

To examine the downstream consequences of MCT1 inhibition on additional aspects of metabolism, we analyzed the ^{1}H NMR spectra of control and AZD3965-treated Raji cell extracts. The data revealed significantly increased levels of branched-chain amino acids (BCAAs), acetate, NADH+NAD+, ribose, succinate, fumarate and ADP+ATP following AZD3965 exposure. Conversely, glutamate and phosphocholine levels were significantly reduced in AZD3965-treated Raji cells relative to controls (Table 1).

The increase in bioenergetic metabolites was further confirmed with ^{31}P NMR, demonstrating increased β-NTP levels in Raji cells (Table 1). ^{31}P NMR also revealed an increase in glycerol 3-phosphate (G 3-P) levels, consistent with earlier reports (7) indicating inhibition of the glycolytic pathway after exposure AZD3965 treatment (Table 1).

We also evaluated changes in the metabolic profile of MCT4+++ HT29 cells, given that they too displayed a build-up (up to 4-fold) in $Lactate_I$ with 500nM AZD3965. ^{1}H NMR analysis revealed increased BCAA, alanine, methionine, glutamine, malate, ribose, creatine +phosphocreatine and ATP+ADP levels in AZD3965-treated relative to control cell extracts (Table 1). Thus, in both MCT4- Raji and MCT4+++ HT29 cells, treatment with AZD3965 at concentrations that led to $Lactate_I$ build-up was associated with improved bioenergetics and increased TCA cycle intermediates. Elevated β-NTP and G 3-P levels were also observed in MCT4+ Hut78 cells treated with 500nM AZD3965 for 24h (up to 129±11% (p=0.02) and 148±12% (p=0.01) of controls, respectively). A bioluminescent assay of ATP confirmed the increased levels following exposure of Raji and Hut78 cells to AZD3965 (Figure S3).

MCT1 inhibition impairs glycolysis and upregulates mitochondrial metabolism

The metabolic basis underlying the improved bioenergetic state and increased TCA cycle intermediates observed with AZD3965 was next investigated by initially assessing mitochondrial abundance using confocal microscopy. MitoTracker® Red staining showed no difference between control and AZD3965-treated Raji cells indicating no changes in functioning mitochondrial density (Figure S4).

Next, we monitored the fate of [1-^{13}C]glucose in Raji cells grown in the presence or absence of drug. ^{13}C NMR analysis of culture media following incubation in [1-^{13}C]glucose indicated that AZD3965 decreased glucose uptake and $Lactate_E$, consistent with reduced glycolytic metabolism (Figure 3A). ^{13}C NMR of intracellular metabolites in treated relative

Europe PMC Funders Author Manuscripts

to control cells revealed a significant increase in [1-^{13}C]glucose, indicating impaired utilization, alongside a substantial rise in [3-^{13}C]lactate, consistent with the rapid blockade of its transport thus reducing export out of cells. Interestingly, these changes were accompanied by significantly elevated ^{13}C-labelling of glutamate at the C4 position, reflecting PDH flux. ^{13}C-labelling of glutamate at the C2 and C3 positions (reflecting PC flux) remained unchanged (Figure 3B and 3C), but given the decreased consumption and incorporation of ^{13}C-glucose into the pathway following treatment, the flux through PC is therefore relatively increased to maintain [2-^{13}C] and [3-^{13}C]glutamate at the same level as in control cells. There was a trend towards a fall in [3-^{13}C]alanine, but this was not statistically significant (p=0.1). Taken together, these results show that AZD3965 treatment blocks lactate transport out of cells, impairs glycolytic activity and increases routing of glucose towards mitochondrial metabolism through oxidative energy producing PDH flux and, to a lesser extent, anaplerotic PC flux.

Increased mitochondrial activity is required to sustain cell survival during MCT1 inhibition

The fact that AZD3965 stimulates mitochondrial oxidative PDH flux leading to increased cellular bioenergy levels suggests acquisition of a metabolic advantage enabling cells to continue growing under MCT1 blockade (Figure 1D). Thus, we hypothesized that stemming this capability, by blocking mitochondrial metabolism, may enhance the anti-proliferative effects of AZD3965.

Growth inhibition data from Raji cells (Figure 4A) revealed that the GI_{50} value of AZD3965 over 72h decreased from 3.91±1.37nM when given as single agent, to 1.03±0.42nM when combined with the mitochondrial complex I inhibitor metformin (n=4, p=0.005), consistent with greater potency. Cell counts over 72h confirmed this effect and indicated that the reduced numbers are due to increased cell death (Figure 4B). The efficacy of AZD3965 was also increased when it was combined with metformin in MCT4+ Hut78 cells although the effects were less pronounced relative to MCT4- Raji cells (Figure 4C).

In neuroblastoma cells harboring *MYCN* amplification and as such representing a solid tumor type expected to be MCT1-dependent (7), AZD3965's therapeutic activity was increased with metformin co-treatment in both MCT4+ Kelly and MCT4- IMR-32 cells (Figure S5A-C). IMR-32 had a very slow doubling time (40-48h compared to 20-24h in Kelly cells), which may account for the relatively smaller changes in cell counts over the 72h treatment. The potentiation of AZD3965's activity by metformin was, at least in Kelly cells, also underpinned by a shift towards mitochondrial metabolism following MCT1 inhibition (as shown by increased fumarate and succinate, Figure S5D). AZD3965 caused a relatively modest increase in $Lactate_I$ in Kelly cells, likely due to MCT4 co-expression (Figure S5A, D).

Furthermore, blockade of pyruvate transport into mitochondria by the mitochondrial pyruvate carrier (MPC) inhibitor UK5099 dose-dependently enhanced the potency of AZD3965 in Raji cells leading to markedly increased cell kill when the two agents were combined relative to when AZD3965 was given alone (Figure 4D). Similar, albeit less profound, effects were also observed in Hut78 after 72h (Figure 4E) and 96h (Figure S6) of

treatment. In both metformin and UK5099 combination treatments of Raji cells, we observed increased PARP cleavage consistent with induction of apoptosis (Figure 4F).

Thus, the AZD3965-induced increase in mitochondrial metabolism is required for maintaining cell survival under therapeutic stress, enabling combination therapy with mitochondrial metabolism inhibitors.

AZD3965 treatment improves tumor bioenergetics detectable non-invasively with *in vivo* ^{31}P NMR spectroscop

Next, to assess the relevance of the *in vitro*-observed changes to *in vivo* tumor metabolism and their potential as non-invasive biomarkers of AZD3965 activity, we evaluated changes in Raji xenograft tumor bioenergetic metabolism using *in vivo* ^{31}P NMR spectroscopy.

Over an acute two-day treatment schedule (Figure 5A), AZD3965 had no significant effect on tumor growth relative to vehicle (percent change in day 2/day 0 tumor volumes was 122±6% *versus* 120±9% for AZD3965 and vehicle groups, respectively (p=0.85). However, after five days of therapy, the treated tumor volumes remained at 123±12% of pre-treatment values (p=0.2) as observed in the acute protocol, consistent with cytostasis, while the vehicle-treated tumors grew up to 171±19% (p=0.036) relative to pre-treatment volumes (Figure 5B).

We observed no differences in % necrotic fractions or perfusion between the 350mm^3 and 450mm^3-sized tumors (representative of the acute vs five-day treatment experiments, Figure S7) and the effect of drug on post-treatment tumor size in the two schedules was also similar indicating that the two settings are comparable.

In vivo ^{31}P NMR spectra obtained pre- and 2 days post-treatment with AZD3965 are shown in Figure 5C where resonances from phosphomonoesters (PMEs), Pi and α-NTP, β-NTP and γ-NTP can be distinguished. Phosphocreatine (PCr) was not observed in most cases and thus was not included in the analysis.

Our results show that compared to day 0, treatment with AZD3965 led to a significant increase in the ratio of β-NTP/total P and β-NTP/Pi up to 178±48% and 198±41, respectively (P=0.01, Figure 5D) in Raji xenograft tumors, indicating an improved bioenergetic state. No significant differences in β-NTP/total P or β-NTP/Pi were detected in vehicle-treated tumors (112±8% and 145±43%, respectively, P≥0.31), Figure 5D. Further, the data revealed no significant changes in tumor pH (as indicated by the relative shift in the α-NTP-Pi resonances) in the AZD3965- or vehicle-treated tumors, indicating that tumor acidification was unaffected (Figure 5E).

High resolution ^{1}H NMR analysis of resected tumor tissue following *in vivo* NMR spectroscopy showed a 1.7-fold increase in lactate levels in the AZD3965-treated relative to the vehicle-treated tumors, confirming MCT1 blockade (Figure 5F). Thus, at the dose and treatment schedule used in our *in vivo* study, AZD3965 caused an increase in tumor lactate accumulation concomitant with improved bioenergetic levels but no changes in tumor acidification. These data indicate that in addition to tumor lactate, bioenergetic status, as determined by ^{31}P NMR measurements of the β-NTP/Pi and β-NTP/total P ratios, could

have potential as an early non-invasive pharmacodynamics biomarker of MCT1 blockade with AZD3965 that precedes gross changes in tumor volumes.

Discussion

Much attention has been focused on disrupting lactate homeostasis for cancer therapy (2–4). As such, understanding the impact of MCT1-targeted drugs on downstream metabolic activity may help identify potential combinatorial strategies as well as metabolic biomarkers for monitoring drug action, which are key for furthering the clinical development of these agents. This is particularly important since MCT1 is ubiquitously expressed (1) and inhibitor administration dose/schedule during the ongoing clinical trials need to be carefully balanced with potential normal tissue toxicity

In this study we focus on lymphoma models as representative of an MCT1-dependent disease (7) and a target patient population within the AZD3965 phase I expansion cohort, with the *MYCN*-amplified MCT4- IMR-32 and MCT4+ Kelly neuroblastoma cell lines representing a solid tumor model expected to be MCT1-dependent (7), and MCT4+++ HT29 cells as a drug resistant model. Using steady state metabolic profiling and flux analyses with hyperpolarized and conventional ^{13}C-labelling, we show that the MCT1 inhibitor AZD3965 blocks lactate transport out of cells with consequences that impact on downstream metabolism and treatment efficacy.

AZD3965 caused a marked time- and concentration-dependent accumulation in $Lactate_I$ that was more pronounced in cells with no or low expression of MCT4, an alternative transporter of lactate that is predictive of resistance to AZD3965 (8). Using hyperpolarized [1-^{13}C]pyruvate, we show that AZD3965 blocks pyruvate-lactate exchange despite the large increases in $Lactate_i$ which are expected to facilitate the process (25). These results are consistent with MCT1-mediated transport of [1-^{13}C]pyruvate being rate-limiting for the reaction (24). Our data also show that inhibition of pyruvate-lactate exchange by AZD3965 is inversely proportional to MCT4 expression and that the action of this agent is bi-directional i.e. it inhibits transport both into and out of cells.

At concentrations that led to accumulation of $Lactate_I$, AZD3965 triggered several other changes in cell metabolism, notably increased TCA cycle metabolic intermediates in MCT4- Raji, MCT4+ Hut78 and Kelly, and MCT4+++ HT29 cells that translated to improved bioenergetics in Raji, Hut78 and HT29 cells. Raji and HT29 cells displayed non-uniform effects on alanine, acetate, glutamate, NADH+NAD+, formate and PC. Whether such differences are related to MCT4 expression remains to be established.

The AZD3965-induced improvement in bioenergetics is of interest since a study carried out with the alternative MCT1 inhibitor SR13800 in Raji cells reported decreased bioenergetic levels and TCA cycle intermediates concomitant with $Lactate_I$ accumulation (7). In contrast, knockout of MCT1 and MCT4 or their molecular chaperone BASIGIN resulted in an increase in $Lactate_I$ pool but no change in ATP levels (26). Similarly, despite the increase in TCA metabolism in Kelly cells in our study, we did not observe a significant increase in

Europe PMC Funders Author Manuscripts

ATP+ADP levels. Thus, the effect of MCT1 inhibition on bioenergetics appears to be context- and drug chemotype-dependent.

Next, and to investigate the metabolic basis underlying the AZD3965-induced changes in bioenergetics, we resorted to [1-^{13}C]glucose metabolic flux analysis. Through ^{13}C NMR analysis of growth media, we found that AZD3965 reduced ^{13}C-glucose uptake and ^{13}C-lactate production (further confirming $Lactate_I$ build-up is due to transport blockade reducing export rather than increased uptake). These effects were concomitant with decreased cellular ^{13}C-glucose utilization possibly reflecting negative feed-back regulation following the rapid and substantial build-up in cellular lactate. Importantly, we also observed a rise in cellular [4-^{13}C]glutamate, indicating increased oxidative PDH flux. Levels of [2-^{13}C]glutamate and [3-^{13}C]glutamate, reflective of PC flux, remained unchanged; however, taking into account the fall in ^{13}C-glucose incorporated into the glycolytic pathway, the data suggest that PC flux is relatively increased to maintain the labeling in [2-^{13}C]glutamate and [3-^{13}C]glutamate at a similar level to the control cells. Thus, AZD3965 stimulates oxidative PDH flux and, concomitantly, a relative increase in anaplerotic PC flux. The flux of pyruvate to alanine appears to be unchanged given the overall fall in ^{13}C label incorporation into the glycolytic pathway, indicating that MCT1 inhibition leads to preferential routing of pyruvate towards mitochondrial metabolism. The upregulated PDH flux is consistent with enhanced oxidative phosphorylation leading to increased bioenergy-related metabolite levels observed with AZD3969, and is in agreement with a previous report showing increased oxygen consumption rates following MCT1 inhibition with AZD3965 (16). The significance of the increased PC flux is potentially multifold as the enzyme can participate in many biosynthetic reactions but one plausible consequence of its activation here is provision of oxaloacetate to support the increased TCA cycle activity (27).

The enhanced mitochondrial metabolism leading to improved cancer cell bioenergetics and biomass production capacity suggests metabolic adaptation to enable improved survival and fitness (28). Indeed, chemoresistance has previously been shown to depend on increased intracellular ATP levels, which can provide metabolic support for key survival pathways (29). We found that while the mitochondrial complex I metformin had little effect on cell counts on its own, it significantly increased the potency of AZD3965. Co-administration of the two agents resulted in increased cell death, indicating that the shift to oxidative mitochondrial metabolism is required to sustain cell survival under MCT1 inhibition. These data are in agreement with recent reports showing that combining AZD3965 with metformin or its analogue phenformin is more effective for tumor targeting than single agent therapy (7,16). Furthermore, blockade of pyruvate mitochondrial transport with the MPC inhibitor UK5099 significantly increased the efficacy of AZD3695 and cell death when the two agents were combined. The increased cell death observed with co-administration of AZD3965+ metformin or AZD3965+UK5099 in Raji cells was concomitant with increased PARP cleavage indicative of apoptosis. Thus, curbing reactivation of mitochondrial metabolism through blockade of pyruvate entry or complex I activity provides a promising strategy for enhancing the anti-tumor effects of AZD3965.

Finally, using *in vivo* ^{31}P NMR spectroscopy of Raji xenograft tumors showed that at a dose and treatment schedule that increased tumor lactate (confirming MCT1 blockade), acute exposure to AZD3965 triggered an increase in β-NTP/Pi and β-NTP/total P, indicating improved tumor bioenergetics, consistent with our *in vitro* observations.

Similar increases in bioenergetic levels have previously been attributed to improved blood flow and tumor reoxygenation following radiation as well as chemotherapy (30–32). The AZD3965-triggered reactivation of oxidative mitochondrial metabolism observed *in vitro* suggests that this mechanism is likely to be a key contributor to the tumor energization observed here although further work is required to assess the effect of the therapy on tumor perfusion.

In vivo ^{31}P NMR spectroscopy is clinically-applicable with many studies reporting its use for evaluating human tumor metabolism (19,33,34). Thus, in addition to direct assessment of tumor lactate with lactate-selective ^{1}H NMR spectroscopy methods (which are also clinically-applicable (35)), the β-NTP/Pi and β-NTP/total P ratios could have potential as metabolic biomarkers for reporting on the action of AZD3965 in tumors. In this regard, and given the relatively low sensitivity of in vivo ^{31}P NMR spectroscopy, good quality spectra are a pre-requisite for obtaining meaningful clinical data,

It is noteworthy that despite triggering an increase in tumor lactate, our data show that AZD3965 treatment had no effect on intracellular tumor pH. One possible explanation for this could be the relatively smaller increase in lactate observed in tumors compared to cells, where others previously reported cell acidification resulting from an increase in the $Lactate_I$ pool following knock out of MCT1/MCT4 or BASIGIN (26). Other potential reasons could be the involvement of additional pH-regulatory mechanisms, such as carbonic anhydrase 9 shown to be upregulated with $Lactate_I$ accumulation (26), although further work is necessary to test this possibility.

Of relevance to monitoring response to therapy, our data also show that AZD3954 blocks hyperpolarized ^{13}C-pyruvate-lactate exchange due primarily to impaired ^{13}C-pyruvate transport following MCT1 inhibition. Although our measurements were not conducted to monitor therapeutic response, but rather to study transport kinetics and further confirm the drug's mechanism of action, the evaluation of hyperpolarized ^{13}C-pyruvate-lactate exchange has shown potential for tumor metabolic imaging in many pre-clinical studies (36) and their clinical feasibility has recently been demonstrated in prostate cancer patients (37,38). When the technology is validated for clinical cancer imaging and becomes more widely available, monitoring hyperpolarized ^{13}C-pyruvate-lactate exchange could provide a complementary biomarker of MCT1 inhibition in tumors *in vivo,* with ^{31}P NMR measurements enabling the assessment of downstream consequences of treatment. Studies such as the one described here are thus of particular value for predicating the design of future clinical trials incorporating much-needed non-invasive biomarkers of drugs targeting cancer metabolism. Following successful completion of a clinical dose finding phase I trial, AZD3965 is now entering the expansion phase of the trial and the data reported here underpin aspects of this trial design and the NMR spectroscopy pharmacodynamic biomarkers included in the protocol.

Europe PMC Funders Author Manuscripts

In summary, we show that MCT1 inhibition with AZD3965 impairs bi-directional monocarboxylate transport, causes build-up of $Lactate_i$ under low/no MCT4 expression and leads to inhibition of glycolytic activity and reactivation of mitochondrial pyruvate metabolism necessary to maintain cell survival. These findings highlight the potential to combine MCT1 inhibitors with mitochondrial-targeted therapy in the clinic and incorporate non-invasive pharmacodynamic magnetic resonance spectroscopy to evaluate drug action in patients.

Supplementary Material

Refer to Web version on PubMed Central for supplementary material.

Acknowledgements

We thank Dr Louise Howell for help with confocal microscopy and the staff of the Biological Services Unit at ICR for animal care and maintenance.

Financial support: M Beloueche-Babari, S Wantuch, T Casals Galobart, M Koniordou, HG Parkes, V Arunan, Y-L Chung, TR Eykyn and MO Leach are supported by a CRUK Centre for Cancer Imaging grant C1090/A16464. We also acknowledge grant C1060/A10334 from CRUK and EPSRC Cancer Imaging Centre in association with the MRC and Department of Health (England), NHS funding to the NIHR Biomedical Research Centre and the Clinical Research Facility in Imaging. MO Leach is a NIHR Emeritus Senior Investigator.

References

1. Halestrap AP. The SLC16 gene family - structure, role and regulation in health and disease. Mol Asp Med. 2013; 34:337–49.
2. Doherty JR, Cleveland JL. Targeting lactate metabolism for cancer therapeutics. J Clin Invest. 2013; 123(9):3685–92. [PubMed: 23999443]
3. Hirschhaeuser F, Sattler UG, Mueller-Klieser W. Lactate: a metabolic key player in cancer. Cancer Res. 2011; 71(22):6921–5. [PubMed: 22084445]
4. Parks SK, Chiche J, Pouyssegur J. Disrupting proton dynamics and energy metabolism for cancer therapy. Nat Rev Cancer. 2013; 13(9):611–23. [PubMed: 23969692]
5. Le Floch R, Chiche J, Marchiq I, Naiken T, Ilc K, Murray CM, et al. CD147 subunit of lactate/H+ symporters MCT1 and hypoxia-inducible MCT4 is critical for energetics and growth of glycolytic tumors. Proc Nat Acad Sci USA. 2011; 108(40):16663–8. [PubMed: 21930917]
6. Baenke F, Dubuis S, Brault C, Weigelt B, Dankworth B, Griffiths B, et al. Functional screening identifies MCT4 as a key regulator of breast cancer cell metabolism and survival. J Pathol. 2015
7. Doherty JR, Yang C, Scott KE, Cameron MD, Fallahi M, Li W, et al. Blocking lactate export by inhibiting the Myc target MCT1 Disables glycolysis and glutathione synthesis. Cancer Res. 2014; 74(3):908–20. [PubMed: 24285728]
8. Polanski R, Hodgkinson CL, Fusi A, Nonaka D, Priest L, Kelly P, et al. Activity of the monocarboxylate transporter 1 inhibitor AZD3965 in small cell lung cancer. Clin Cancer Res. 2014; 20(4):926–37. [PubMed: 24277449]
9. Bola BM, Chadwick AL, Michopoulos F, Blount KG, Telfer BA, Williams KJ, et al. Inhibition of monocarboxylate transporter-1 (MCT1) by AZD3965 enhances radiosensitivity by reducing lactate transport. Mol Cancer Ther. 2014; 13(12):2805–16. [PubMed: 25281618]
10. Beloueche-Babari M, Workman P, Leach MO. Exploiting tumor metabolism for non-invasive imaging of the therapeutic activity of molecularly targeted anticancer agents. Cell Cycle. 2011; 10(17)
11. Tunariu N, Kaye SB, DeSouza NM. Functional imaging: what evidence is there for its utility in clinical trials of targeted therapies? Brit J Cancer. 2012; 106(4):619–28. [PubMed: 22281664]

Europe PMC Funders Author Manuscripts

12. Brindle KM, Bohndiek SE, Gallagher FA, Kettunen MI. Tumor imaging using hyperpolarized ^{13}C magnetic resonance spectroscopy. Magn Reson Med. 2011; 66(2):505–19. [PubMed: 21661043]
13. Falck Miniotis M, Arunan V, Eykyn TR, Marais R, Workman P, Leach MO, et al. MEK1/2 inhibition decreases lactate in BRAF-driven human cancer cells. Cancer Res. 2013; 73(13):4039–49. [PubMed: 23639941]
14. Ward CS, Venkatesh HS, Chaumeil MM, Brandes AH, Vancriekinge M, Dafni H, et al. Noninvasive detection of target modulation following phosphatidylinositol 3-kinase inhibition using hyperpolarized ^{13}C magnetic resonance spectroscopy. Cancer Res. 2010; 70(4):1296–305. [PubMed: 20145128]
15. Al-Saffar NM, Marshall LV, Jackson LE, Balarajah G, Eykyn TR, Agliano A, et al. Lactate and choline metabolites detected in vitro by nuclear magnetic resonance spectroscopy are potential metabolic biomarkers for PI3K inhibition in pediatric glioblastoma. PloS One. 2014; 9(8):e103835. [PubMed: 25084455]
16. Hong CS, Graham NA, Gu W, Espindola Camacho C, Mah V, Maresh EL, et al. MCT1 Modulates Cancer Cell Pyruvate Export and Growth of Tumors that Co-express MCT1 and MCT4. Cell Rep. 2016; 14(7):1590–601. [PubMed: 26876179]
17. Beloueche-Babari M, Arunan V, Troy H, te Poele RH, te Fong AC, Jackson LE, et al. Histone deacetylase inhibition increases levels of choline kinase alpha and phosphocholine facilitating noninvasive imaging in human cancers. Cancer Res. 2012; 72(4):990–1000. [PubMed: 22194463]
18. Workman P, Aboagye EO, Balkwill F, Balmain A, Bruder G, Chaplin DJ, et al. Guidelines for the welfare and use of animals in cancer research. Brit J Cancer. 2010; 102(11):1555–77. [PubMed: 20502460]
19. Rata M, Giles SL, deSouza NM, Leach MO, Payne GS. Comparison of three reference methods for the measurement of intracellular pH using ^{31}P MRS in healthy volunteers and patients with lymphoma. NMR Biomed. 2014; 27(2):158–62. [PubMed: 24738141]
20. Beloueche-Babari M, Box C, Arunan V, Parkes HG, Valenti M, De Haven Brandon A, et al. Acquired resistance to EGFR tyrosine kinase inhibitors alters the metabolism of human head and neck squamous carcinoma cells and xenograft tumours. Brit J Cancer. 2015; 112(7):1206–14. [PubMed: 25742484]
21. Beloueche-Babari M, Jackson LE, Al-Saffar NM, Eccles SA, Raynaud FI, Workman P, et al. Identification of magnetic resonance detectable metabolic changes associated with inhibition of phosphoinositide 3-kinase signaling in human breast cancer cells. Mol Cancer Ther. 2006; 5(1): 187–96. [PubMed: 16432178]
22. Hill DK, Orton MR, Mariotti E, Boult JK, Panek R, Jafar M, et al. Model free approach to kinetic analysis of real-time hyperpolarized ^{13}C magnetic resonance spectroscopy data. PloS One. 2013; 8(9):e71996. [PubMed: 24023724]
23. Venkatesh HS, Chaumeil MM, Ward CS, Haas-Kogan DA, James CD, Ronen SM. Reduced phosphocholine and hyperpolarized lactate provide magnetic resonance biomarkers of PI3K/Akt/mTOR inhibition in glioblastoma. Neuro Oncol. 2012; 14:315–25. [PubMed: 22156546]
24. Harris T, Eliyahu G, Frydman L, Degani H. Kinetics of hyperpolarized ^{13}C1-pyruvate transport and metabolism in living human breast cancer cells. Proc Nat Acad Sci USA. 2009; 106(43): 18131–6. [PubMed: 19826085]
25. Witney TH, Kettunen MI, Brindle KM. Kinetic modeling of hyperpolarized ^{13}C label exchange between pyruvate and lactate in tumor cells. J Biol Chem. 2011; 286(28):24572–80. [PubMed: 21596745]
26. Marchiq I, Le Floch R, Roux D, Simon MP, Pouyssegur J. Genetic disruption of lactate/H+ symporters (MCTs) and their subunit CD147/BASIGIN sensitizes glycolytic tumor cells to phenformin. Cancer Res. 2015; 75(1):171–80. [PubMed: 25403912]
27. Jitrapakdee S, St Maurice M, Rayment I, Cleland WW, Wallace JC, Attwood PV. Structure, mechanism and regulation of pyruvate carboxylase. Biochem J. 2008; 413(3):369–87. [PubMed: 18613815]
28. Caino MC, Altieri DC. Molecular Pathways: Mitochondrial Reprogramming in Tumor Progression and Therapy. Clin Cancer Res. 2016; 22(3):540–5. [PubMed: 26660517]

29. Zhou Y, Tozzi F, Chen J, Fan F, Xia L, Wang J, et al. Intracellular ATP levels are a pivotal determinant of chemoresistance in colon cancer cells. Cancer Res. 2012; 72(1):304–14. [PubMed: 22084398]
30. Mahmood U, Alfieri AA, Thaler H, Cowburn D, Koutcher JA. Radiation dose-dependent changes in tumor metabolism measured by ^{31}P nuclear magnetic resonance spectroscopy. Cancer Res. 1994; 54(18):4885–91. [PubMed: 8069854]
31. Street JC, Alfieri AA, Traganos F, Koutcher JA. In vivo and ex vivo study of metabolic and cellular effects of 5-fluorouracil chemotherapy in a mouse mammary carcinoma. Magn Reson Imaging. 1997; 15(5):587–96. [PubMed: 9254003]
32. Tozer GM, Bhujwalla ZM, Griffiths JR, Maxwell RJ. Phosphorus-31 magnetic resonance spectroscopy and blood perfusion of the RIF-1 tumor following X-irradiation. Int J Radiat Oncol Biol Phys. 1989; 16(1):155–64. [PubMed: 2912937]
33. Arias-Mendoza F, Payne GS, Zakian KL, Schwarz AJ, Stubbs M, Stoyanova R, et al. In vivo ^{31}P MR spectral patterns and reproducibility in cancer patients studied in a multi-institutional trial. NMR Biomed. 2006; 19(4):504–12. [PubMed: 16763965]
34. Wijnen JP, Scheenen TW, Klomp DW, Heerschap A. ^{31}P magnetic resonance spectroscopic imaging with polarisation transfer of phosphomono- and diesters at 3 T in the human brain: relation with age and spatial differences. NMR Biomed. 2010; 23(8):968–76. [PubMed: 20669234]
35. Harris LM, Tunariu N, Messiou C, Hughes J, Wallace T, DeSouza NM, et al. Evaluation of lactate detection using selective multiple quantum coherence in phantoms and brain tumours. NMR Biomed. 2015; 28(3):338–43. [PubMed: 25586623]
36. Brindle KM. Imaging metabolism with hyperpolarized ^{13}C-labeled cell substrates. J Am Chem Soc. 2015; 137(20):6418–27. [PubMed: 25950268]
37. Wilson DM, Kurhanewicz J. Hyperpolarized ^{13}C MR for molecular imaging of prostate cancer. J Nucl Med. 2014; 55(10):1567–72. [PubMed: 25168625]
38. Nelson SJ, Kurhanewicz J, Vigneron DB, Larson PE, Harzstark AL, Ferrone M, et al. Metabolic imaging of patients with prostate cancer using hyperpolarized [1-^{13}C]pyruvate. Sci Transl Med. 2013; 5(198):198ra08.

Europe PMC Funders Author Manuscripts

Europe PMC Funders Author Manuscripts

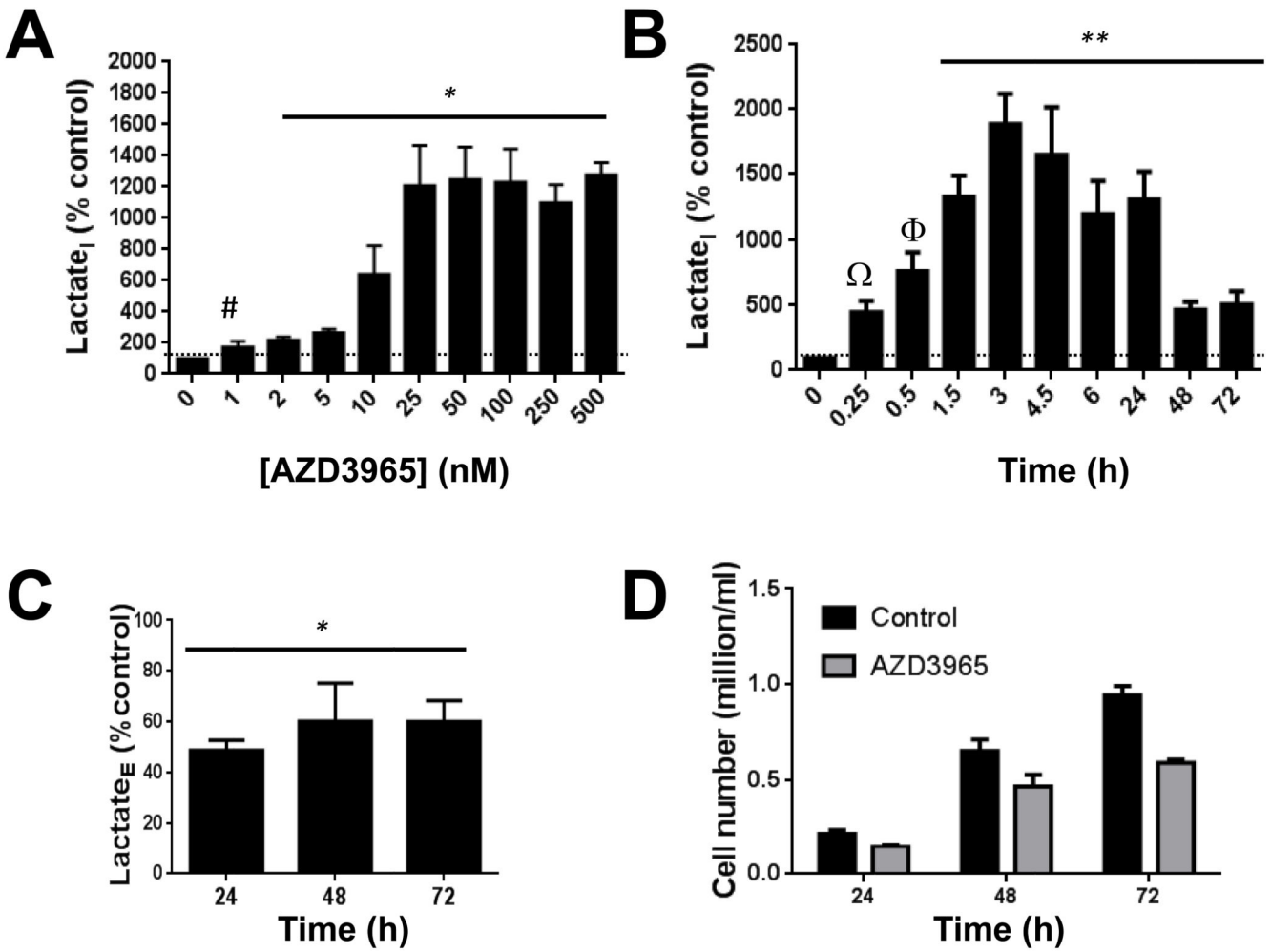

Figure 1. Time- and concentration-dependent effects of AZD3965 on intracellular and extracellular lactate levels and cell counts in MCT4- Raji human lymphoma cells.

A) Concentration-dependent accumulation in $Lactate_I$ in Raji cells treated for 24h with AZD3965. **B)** Time dependent-changes in $Lactate_I$ in 25nM AZD3965-treated Raji cells relative to same time point controls. **C)** Decreased $Lactate_E$ in Raji cells following exposure to AZD3965 (25nM) for the indicated durations. **D)** AZD3965 treatment (25nM) reduces but does not totally halt Raji cell proliferation over 72h. *: $p<0.05$, **: $P\leq0.03$, #, $P=0.12$, Ω: $P=0.07$, Φ: $P=0.06$. Dashed line represents the 100% control level.

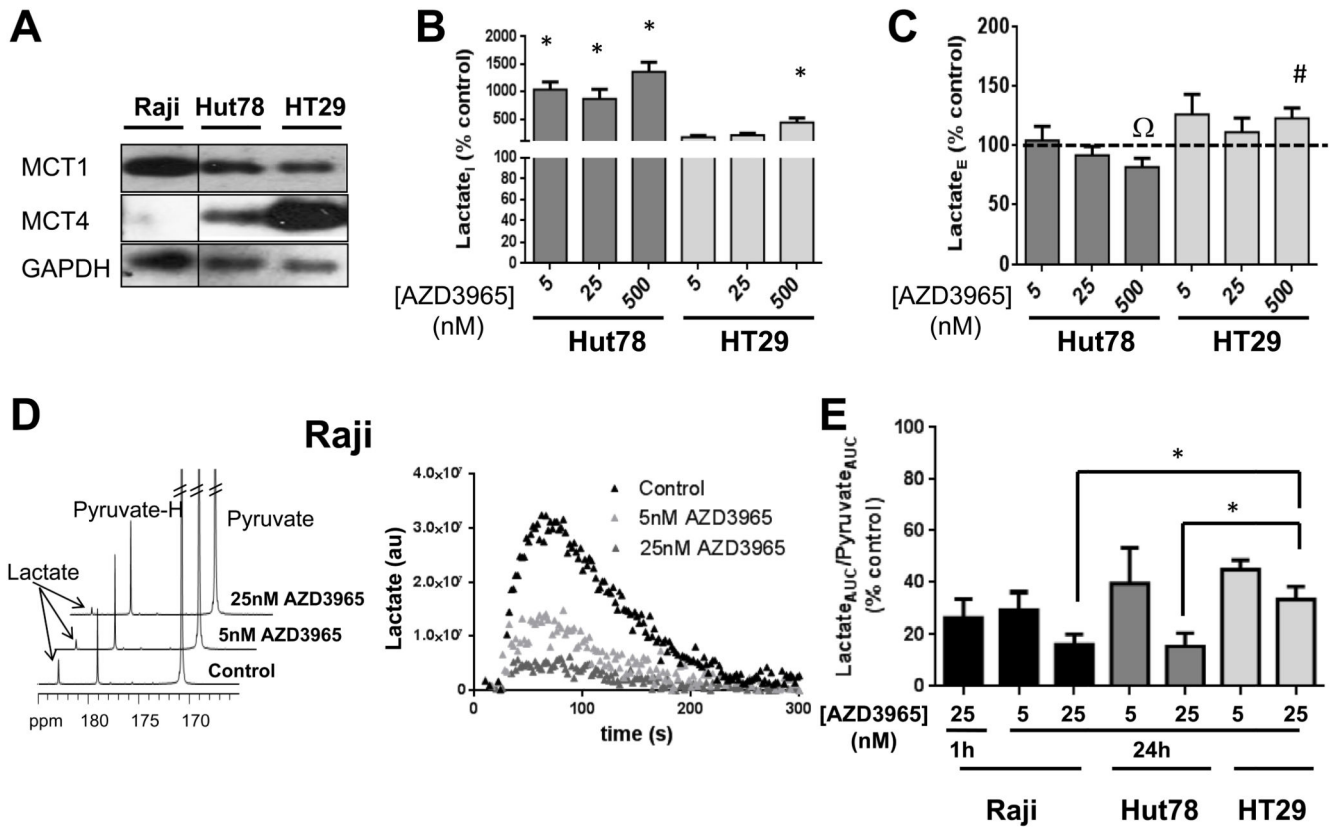

Figure 2. AZD3965 effects on monocarboxylate influx and efflux in human cancer cells harboring varying MCT4 expression levels.

A) Western blots showing baseline MCT1 and MCT4 expression in Raji, Hut78 and HT29 human cancer cells. **B)** The effect of AZD3965 on Lactate$_I$ and **C)** Lactate$_E$ levels in MCT4+ Hut78 and MCT4+++ HT29 cells. **D)** ^{13}C NMR spectra and time series integrals showing the changes in hyperpolarized ^{13}C-lactate signal following incubation of control, 5nM and 25nM AZD3965-treated Raji in hyperpolarized ^{13}C-pyruvate. **E)** Summary of changes in of ^{13}C-pyruvate-lactate exchange (determined by Lactate$_{AUC}$/Pyruvate$_{AUC}$) resulting from inhibition of ^{13}C-pyruvate uptake by AZD3965 in MCT4- Raji, MCT4+ Hut78 and MCT4+++ HT29 human cancer cells. *: $P \leq 0.04$, #: $P = 0.077$, Ω: $P = 0.067$. Dashed line represents the 100% control level.

Europe PMC Funders Author Manuscripts

Europe PMC Funders Author Manuscripts

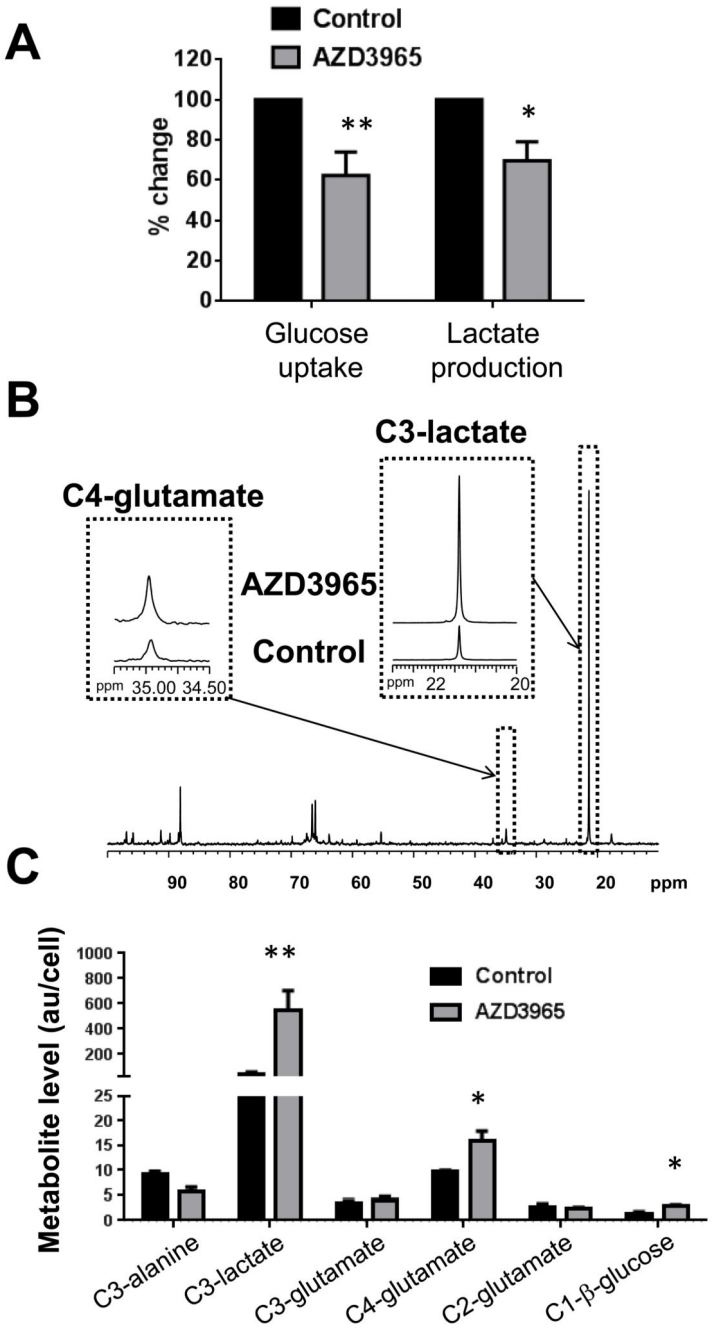

Figure 3. MCT1 inhibition with AZD3965 impairs glycolytic activity and increases mitochondrial pyruvate metabolism.

A) Extracellular metabolite analysis of [1-^{13}C]glucose labelled media from Raji cells show decreased glucose uptake and lactate production following exposure to AZD3965 (25nM, 6h). **B)** ^{13}C NMR spectra illustrating the changes in [3-^{13}C]lactate and [4-^{13}C]glutamate signals in AZD3965-treated compared to control Raji cells incubated in [1-,^{13}C]glucose for 6h. **C)** Intracellular [1-^{13}C]glucose flux analysis in Raji cells showing increased

[4-^{13}C]glutamate (PDH flux) concomitant with accumulation of [3-^{13}C]lactate and [1-^{13}C]glucose following AZD3965 treatment. **: P≤0.01, *: P<0.02.

Europe PMC Funders Author Manuscripts

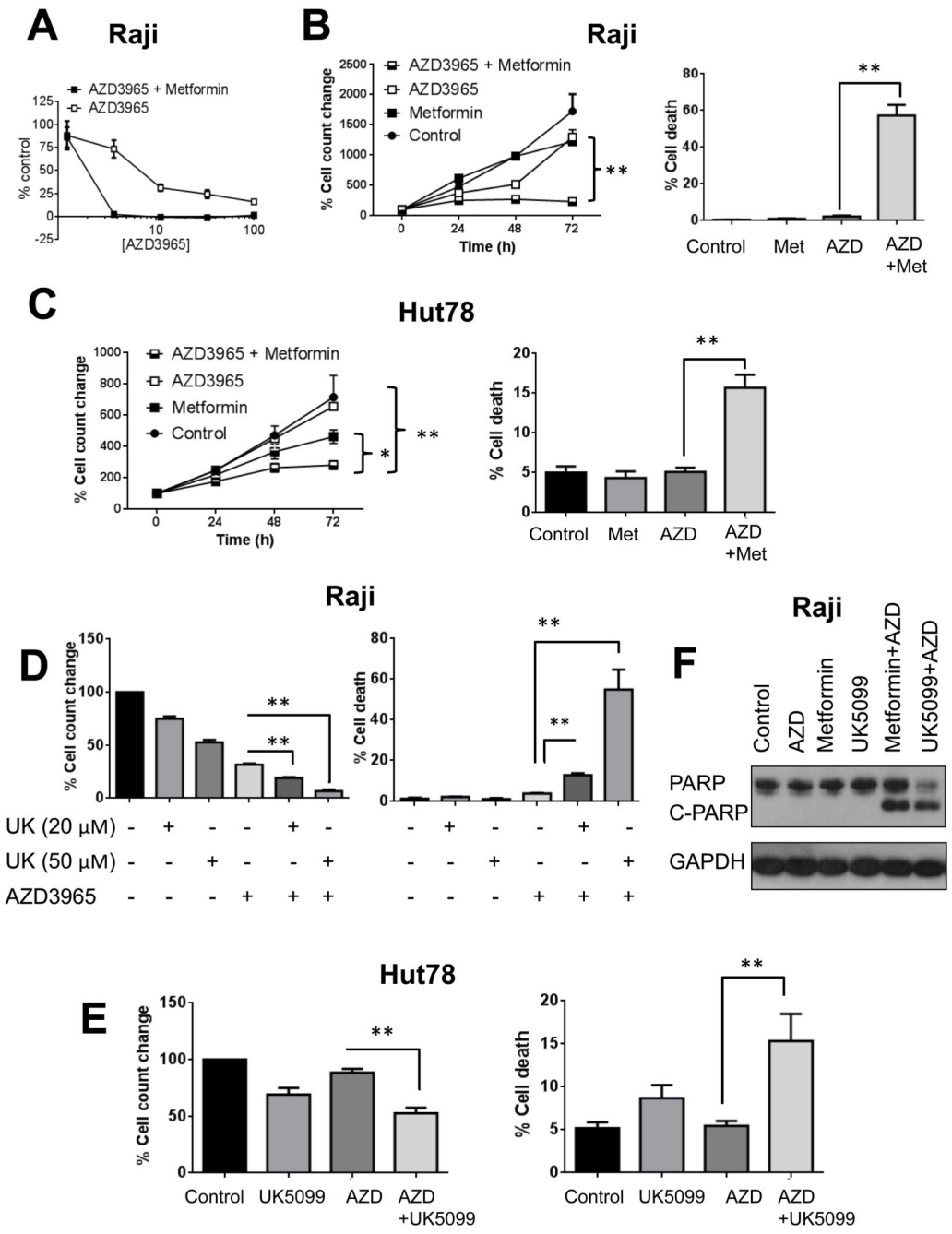

Figure 4. Impairing mitochondrial metabolism increases sensitivity to AZD3965.

A) Cell growth inhibition data showing that blockade of oxidative mitochondrial metabolism by complex I inhibitor metformin (1mM) increases the potency of AZD3965 (72h exposure). **B)** Cell count and viability data showing that inhibition with metformin (1mM, Met) prevents the continued cell growth observed with AZD3965 alone (25nM, AZD) and promotes cell kill in Raji cells as indicated by trypan blue exclusion. C) Cell counts showing that inhibition with metformin (1mM) enhances the anti-proliferative effects of AZD3965 (25nM) and increases cell death (as indicated by trypan blue staining) in Hut78 cells. **D)**

Europe PMC Funders Author Manuscripts

Cell count and % viability data showing that inhibition of MPC with UK5099 (UK) enhances the efficacy of AZD3965 (25nM, 72h) leading to increased cell death in Raji cells. **E)** Cell counts and % viability data showing that co-treatment with the MPC inhibitor UK5099 (50 μM) enhances the anti-proliferative effects of AZD3965 (AZD 25nM, 72h) and increases cell death (as indicated by trypan blue staining) in Hut78 cells. **F)** Western blots showing increased PARP cleavage (C-PARP/PARP) in Raji cells treated for 72h with a combination of AZD3965 (25nM, AZD)+Metformin (1mM, Met) or UK5099 (50μM) relative to single agent therapy.*P<0.02, **: P<0.01.

Europe PMC Funders Author Manuscripts

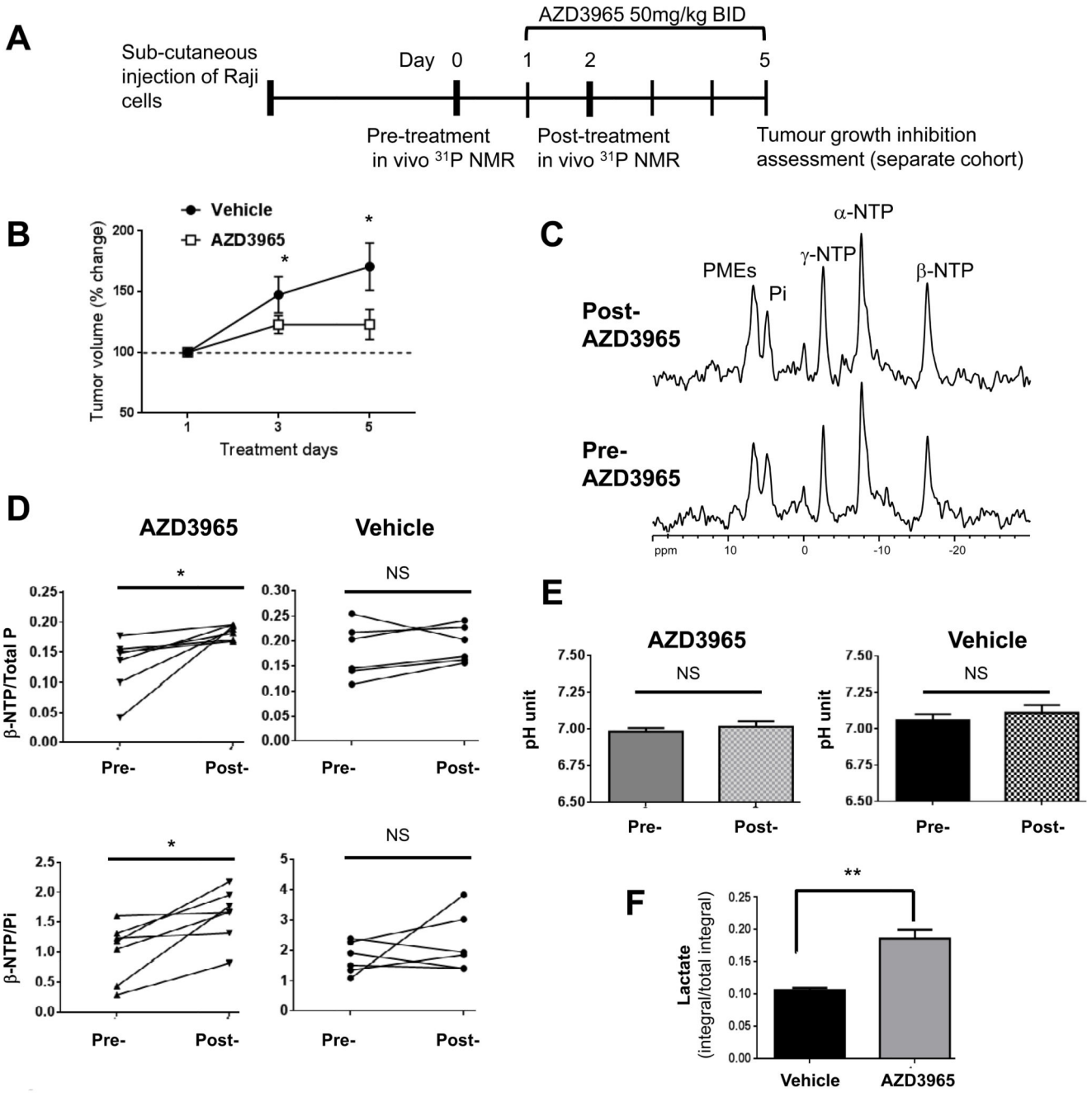

Figure 5. AZD3965 treatment leads to improved bioeneregetics in Raji xenograft tumors but no changes in tumor pH as observed by *in vivo* ^{31}P NMR spectroscopy.

A) Schematic of the *in vivo* study protocol. **B)** Changes in Raji xenograft tumor growth following administration of AZD3965 (50mg/kg twice daily) over 5 days. **C)** *in vivo* ^{31}P NMR spectra obtained from Raji xenograft tumors showing improved tumor bioenergetics (β-NTP/total P and β-NTP/Pi) following 2 days of AZD3965 treatment. **D)** Changes in the ratios of β-NTP/total P and β-NTP/Pi detected by *in vivo* ^{31}P NMR spectroscopy following vehicle or AZD3965 treatment in Raji xenograft tumors. **E)** Changes in tumor pH following

vehicle or AZD3965 treatment as measured by *in vivo* ^{31}P NMR spectroscopy. **F)** Lactate levels in vehicle- and AZD3965-treated tumors measured by *ex vivo* ^{1}H NMR analysis of resected tumors confirm MCT1 inhibition. **: P=0.001, *: P≤0.03, NS: P≥0.36.

Europe PMC Funders Author Manuscripts

Europe PMC Funders Author Manuscripts

Table 1

Changes in ^{1}H and ^{31}P NMR-detectable metabolite levels observed with the MCT1 inhibitor AZD3965 in Raji and HT29 human cancer cells

Treatment	**AZD3965 (500nM, 24h)**			
Cell line	**Raji**	***P***	**HT29**	***P***
^{1}H NMR				
Lactate	1480±296	*0.002*	438±81	*0.025*
BCAA	154±11	*0.001*	152±7	*0.008*
Alanine	91±7	*0.34*	161±9	*0.003*
Acetate	159±9	*0.001*	101±8	*0.44*
Methionine	ND	-	196±27	*0.02*
Glutamate	57±9	*0.002*	128±13	*0.12*
Glutamine	ND	-	154±11	*0.013*
Succinate	219±39	*0.043*	ND	-
Glutathione	101±21	*0.82*	117±4	*0.082*
Malate	144±22	*0.078*	154±15	*0.033*
Cr+PCr	ND	-	131±7	*0.004*
PC	35±7	*0.001*	112±7	*0.42*
GPC	ND	-	91±4	*0.11*
Myo-inositol	108±18	*0.67*	115±17	*0.54*
NADH+NAD+	185±32	*0.028*	105±2	*0.059*
Ribose	148±6	*0.002*	129±6	*0.012*
Fumarate	328±37	*0.033*	174±39	*0.088*
ATP+ADP	142±10	*0.011*	137±9	*0.026*
Formate	140±3	*0.001*	97±8	*0.53*
^{31}P NMR				
PC	24±3	*0.01*	105±11	*0.68*
β-NTP	160±11	*0.03*	133±13	*0.06*
G 3-P	195±16	*0.025*	ND	-

Metabolites are expressed as % of control content per cell. ND: not detectable. N≥3. Abbreviations: BCAA: branched-chain amino acids, Cr+PCr: creatine+phosphocreatine, G 3-P: glycerol 3-phosphate, PC: phosphocholine.